ACS OMEGA

http://pubs.acs.org/journal/acsodf

Article

# Mechanistic Investigation of Xuebijing for Treatment of Paraquat-Induced Pulmonary Fibrosis by Metabolomics and Network Pharmacology

Tongtong Wang,[‖] Sha Li,[‖] Yangke Wu, Xiao Yan, Yiming Zhu, Yu Jiang, Feiya Jiang, and Wen Liu*

Cite This: *ACS Omega* 2021, 6, 19717−19730

Read Online

ACCESS | Metrics & More | Article Recommendations

**ABSTRACT:** After paraquat (PQ) poisoning, it is difficult to accurately diagnose patients' condition by only measuring their blood PQ concentration. Therefore, it is important to establish an accurate method to assist in the diagnosis of PQ poisoning, especially in the early stages. In this study, a gas chromatography−mass spectrometry (GC−MS) metabonomics strategy was established to obtain metabolite information. A random forest algorithm was used to search for potential biomarkers of PQ poisoning, and data mining and network pharmacological analysis were used to evaluate the active components, drug−disease targets, and key pathways of Xuebijing (XBJ) injection in the treatment of PQ-induced pulmonary fibrosis. Targets from the network pharmacology analysis and metabolites from plasma metabolomics were jointly analyzed to select crucial metabolic pathways. Finally, molecular docking technology and in vitro experiments were used to verify the pathway targets to further reveal the potential mechanisms underlying the antipulmonary fibrosis effect of XBJ. Metabonomics studies showed that L-valine, glycine, citric acid, D-mannose, D-galactose, maltose, L-tryptophan, and arachidonic acid contributed more to the differentiation of different groups than other metabolites. Compared with the control group, the PQ poisoning group had higher levels of L-valine, glycine, citric acid, L-tryptophan, and arachidonic acid, and lower levels of D-mannose, D-galactose, and maltose. After treatment with XBJ injection, the relative levels of these metabolites were reversed. The network pharmacological analysis screened a total of 180 targets, mainly involving multiple signaling pathways and metabolic pathways, which jointly played an antipulmonary fibrosis effect. Based on the combined analysis of 180 targets and 8 different metabolites, arachidonic acid metabolism was selected as the key metabolic pathway. Molecular docking analysis showed that the XBJ compound had strong binding activity with the target protein. Western blot results showed that XBJ injection could reduce the inflammatory response by downregulating the expressions of p-p65, p-IKB$\alpha$, and p-IKK$\beta$, thus inhibiting the development of PQ-induced pulmonary fibrosis. In summary, the combined results from metabolomics and network pharmacology studies showed that Xuebijing has the characteristics of multitarget, multichannel, and multicomponent action in the treatment of pulmonary fibrosis caused by PQ.

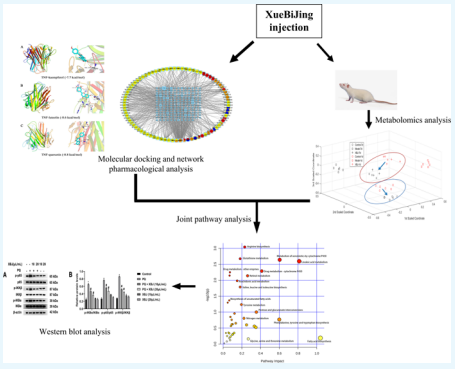


## 1. INTRODUCTION

Paraquat (PQ) is a nonselective and broad-spectrum highly effective herbicide that leaves few residues and creates little pollution. It is widely used in agricultural production around the world, and although it is relatively safe for routine agricultural use, it is highly toxic to humans and animals.[1] For humans, the lethal dose is only 7−8 mL. Every year, many cases of poisoning and death are reported, particularly in developing countries. PQ can cause acute lung, liver, and kidney damage and failure. Lungs are the main target organ of PQ and it accumulates in lung tissue after poisoning, which results in progressive pulmonary fibrosis in patients and causes respiratory failure and eventual death.[1,2]

To date, clinical studies have suggested that blood purification, hemodialysis, and administration of antioxidants, cyclophosphamide, and corticosteroid are effective methods for PQ poisoning treatment. The mortality can be effectively reduced if treatment is initiated within 2−4 h of poisoning, especially using hemoperfusion.[3−5] However, the effectiveness of conventional treatments is extremely limited. A challenge with diagnosis of PQ poisoning is that a routine clinical diagnosis is mainly based on the blood PQ concentration. However, PQ is absorbed poorly from the stomach and small intestine and can be distributed to all organs in the body within 5 h, making it difficult to detect PQ in blood if the poisoning occurs more than 5 h before sampling.[6] In most cases, patients cannot provide a clear history of PQ exposure, such as the

Received: May 5, 2021
Accepted: July 12, 2021
Published: July 20, 2021

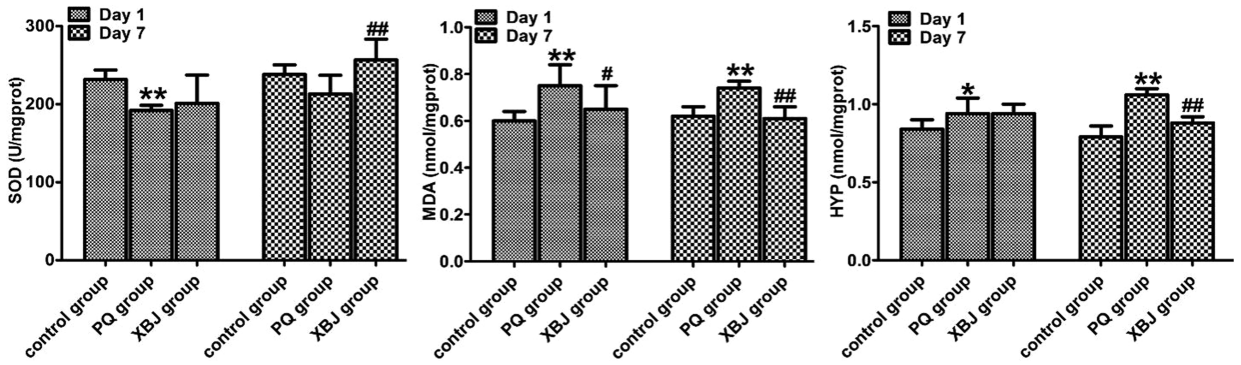


**Figure 1.** Effect of XBJ on the changes of various biochemical indicators after PQ poisoning. Each value represents the mean ± standard deviation (SD) of three independent experiments; * represents the comparison between PQ and control groups,* represents $P < 0.05$, ** represents $P < 0.01$, # represents the comparison between XBJ and PQ groups, # represents $P < 0.05$, and ## represents $P < 0.01$.

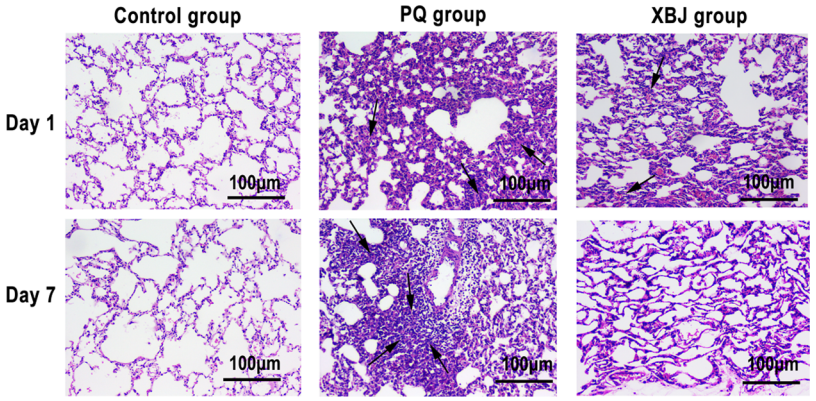


**Figure 2.** Pathological changes in rat lung tissue were observed under a light microscope. Black arrows: Morphological damage. Representative images of hematoxylin and eosin (H&E)-stained lung sections from the three experimental groups (magnification: 200×).

exposure time or dose, which increases the difficulty of clinical diagnosis. Therefore, it is important to establish a method to help with diagnosis of PQ poisoning, especially in the early stages when treatment can be most effective.

Some Chinese medicines are widely used for clinical treatment of PQ poisoning. Traditional Chinese medicines (TCM) combined with blood perfusion for treatment of PQ poisoning can effectively relieve organ dysfunction and prevent pulmonary fibrosis.[7] Xuebijing (XBJ) injection is a medicine prepared from extracts of *Carthamus tinctorius*, *Paeonia lactiflora* roots, ligusticum chuanxiong rhizomes, *Angelica sinensis* roots, and *Salvia miltiorrhiza* roots. XBJ can scavenge oxygen free radicals, protect vascular endothelium, and act as an anti-inflammatory mediator and antagonistic endotoxin. It has been widely used in the treatment of patients with infection and severe poisoning, where it reduces the ultrastructural damage of lung tissue and prevents pulmonary fibrosis.[8−13] XBJ also reduces the risk of death in patients with acute PQ poisoning by improving vital organ function and prolonging survival.[14] Presently, XBJ is recommended by the National Health Commission of the People's Republic of China to treat 2019-novel coronavirus-related pneumonia.[15] Network pharmacology is a systems analysis method based on networks of disease, gene, protein target, and drug interactions. It combines systems biology and computational biology to elucidate the mechanism of drug action from a holistic, synergistic, and dynamic perspective. It is in line with the holistic view of traditional Chinese medicine (TCM) and the characteristics of syndrome differentiation and treatment, which provides an important method for TCM formula analysis.[16,17]

In recent years, metabolomics has been widely applied to various fields, including nutrition, pharmaceutical research, and toxicity studies because it can be used to measure important metabolites quickly and easily, and it is especially useful for investigating systematic metabolic responses to toxins and drugs.[18−20] Gas chromatography−mass spectrometry (GC−MS) is a conventional technique widely used for nontargeted metabolomics, which has good separation, high sensitivity, and can be both qualitative and quantitative.[18,19,21] Deng et al. developed a serum metabolomics method using GC−MS and orthogonal partial least-squares discriminant analysis to evaluate the effect of chronic hydrogen sulfide poisoning in rats.[18] They concluded that more metabolomics studies involving long-term evaluation of large numbers of animal models and human patients with chronic $H_2S$ poisoning is required to link the results with clinical indicators or biomarkers in blood. Wen et al. developed a serum metabolomics method using GC−MS to evaluate the effects of acute PQ poisoning in rats. Their results indicated that the exploration of biomarkers by GC−MS metabolomics methods will be useful to elucidate the mechanism of PQ poisoning.[20]

In this study, a GC−MS metabolomics approach was developed for evaluating the metabolic status after PQ poisoning. Interactions between key compounds and disease targets were studied using network pharmacological methods and molecular docking pairs. Additionally, the interaction between selected compounds and proteins was verified by the


https://doi.org/10.1021/acsomega.1c02370
ACS Omega 2021, 6, 19717−19730

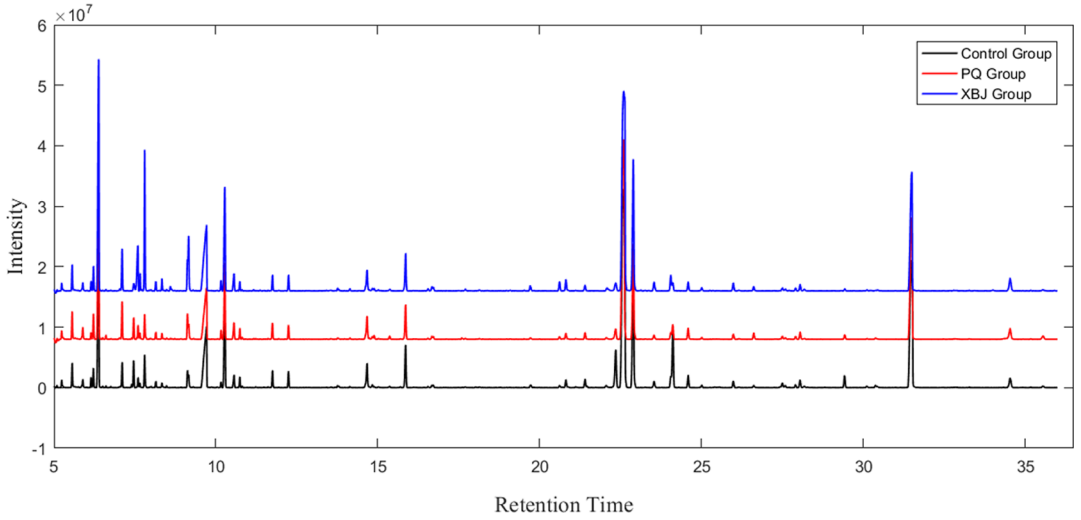


**Figure 3.** Total ion chromatograms (TIC) of different sample groups.

western blot analysis. Results of the current study supply the theoretical and experimental basis for the treatment of PQ-induced pulmonary fibrosis with XBJ.

## 2. RESULTS

**2.1. Pathological Changes Induced by XBJ Injection against Paraquat.** Three indices, superoxide dismutase (SOD), malondialdehyde (MDA), and hydroxyproline (HYP), were used to monitor the animal models and treatment process (Figure 1). After administration of PQ, SOD activity in the tissue homogenate was lower than that in the control group ($P < 0.01$). In contrast, MDA and HYP contents in the PQ group were significantly higher than those in the control group ($P < 0.01$). These results indicated that the PQ model was successful established. Pathological alterations in the lungs in the three groups are shown in Figure 2. The lung tissue in the control group showed no obvious pathological changes. In contrast, the lung tissue in the PQ group showed extensive morphological injury, contained interstitial edema, alveolar hemorrhage, alveolar wall thickening, inflammatory cell infiltration, and even tissue destruction. However, after treatment with XBJ, these symptoms were attenuated as shown by the changes in the activity of SOD, MDA, and HYP contents, and pathological changes.

**2.2. Metabolomics Analysis.** Total ion chromatograms (TIC) for the different groups are shown in Figure 3. The serum metabolites in the three groups were essentially the same, but the contents varied. Forty-six common metabolites (Table 1) were identified from the chromatographic profiles, including amino acids, sugars, fatty acids, and organic acids.

**2.3. Multivariate Statistical Analysis and Identification of Metabolites for Differentiating Groups.** After qualitative and quantitative analysis of all endogenous metabolites in the rat sera, the metabolites were input into MATLAB (MathWorks Co.) software for analysis. The random forest (RF) algorithm was used to analyze the metabolic characteristics of different groups on different days (Figure 4). The classification plot showed a distinct separation between the control group and PQ group. On the first day after treatment, the PQ group was not clearly distinguished from the XBJ group, which meant that the treatment effect was not obvious at this time. By contrast, after 7 days, the PQ and XBJ groups were obviously separated. The XBJ group was closer to the control group than the PQ group, indicating that XBJ injection had anti-PQ toxicity effects.

Variable importance in projection (VIP) parameters have been widely used for biomarker screening and can indirectly reflect the correlations between metabolites and diseases. In the classification process, the RF algorithm calculates the variable importance of each metabolite, which can facilitate the discovery of potential biomarkers for diagnosis of PQ poisoning and estimation of therapeutic effects. In a graph of the variable importance of each metabolite from the RF algorithm (Figure 5), several metabolites showed consistent trends for distinguishing the PQ group from the control group. The metabolites with high variable importance were L-valine, glycine, citric acid, D-mannose, D-galactose, maltose, L-tryptophan, and arachidonic acid. When *t*-tests were performed on these metabolites (Table 2), compared with the control group, the levels of L-valine, glycine, citric acid, L-tryptophan, and arachidonic acid in the PQ group increased and the levels of D-mannose, D-galactose, and maltose decreased. After treatment with XBJ, the relative levels of these metabolites were reversed.

**2.4. Metabolic Pathway Analysis of PQ Poisoning.** Potential biomarkers with significant group differences were introduced into MetaboAnalyst to explore the metabolic pathways using the Kyoto Gene and Genomic Encyclopedia (KEGG). The metabolic pathway information on PQ poisoning and XBJ treatment is displayed in Figure 6. The main metabolic pathways include aminoacyl-tRNA, valine, leucine, and isoleucine biosynthesis, and glyoxylate, dicarboxylate, starch, sucrose, and arachidonic acid metabolism.

**2.5. Network Pharmacology Analysis.** A total of 125 active ingredients of XBJ were collected by the TCMSP database, including 29 active ingredients of *P. lactiflora*, 7 active ingredients of ligusticum chuanxiong, 2 active ingredients of *A. sinensis*, 65 active ingredients of *S. miltiorrhiza*, and 22 active ingredients of *C. tinctorius*. At the same time, 180 potential targets related to XBJ in the treatment of pulmonary fibrosis were obtained, as shown in Figure 7. Through Cytoscape 3.7.0 software, the network of "active ingredient−target−disease" was constructed with 265 nodes and 866 edges (Figure 8). Intersection genes (180) were imported into the STING database, the protein−protein interaction (PPI) network map


https://doi.org/10.1021/acsomega.1c02370
*ACS Omega* 2021, 6, 19717−19730

**Table 1. Qualitative and Quantitative Analysis of Metabolic Profiles of PQ, XBJ, and Healthy Control Groups**

| | | | 1 day | | | 7 days | | |
|---|---|---|---|---|---|---|---|---|
| peak no. | metabolite | $R_t$ (min) | control | PQ | XBJ | control | PQ | XBJ |
| 1 | D-lactic acid | 6.378 | 6.299 ± 0.5591 | 6.1781 ± 0.7141 | 6.5802 ± 0.8294 | 5.912 ± 0.5988 | 5.9154 ± 0.5102 | 6.277 ± 0.4949 |
| 2 | glycolic acid | 6.601 | 0.0398 ± 0.0085 | 0.0479 ± 0.011 | 0.0397 ± 0.0068 | 0.0496 ± 0.0035 | 0.0552 ± 0.0044 | 0.041 ± 0.0045 |
| 3 | L-alanine | 7.104 | 0.8403 ± 0.0569 | 0.7367 ± 0.0307 | 0.816 ± 0.0589 | 0.7267 ± 0.0642 | 0.8702 ± 0.0563 | 0.815 ± 0.0362 |
| 4 | oxalic acid | 7.6571; 7.806 | 0.8252 ± 0.0785 | 1.1035 ± 0.0375 | 1.1247 ± 0.0904 | 0.6228 ± 0.0412 | 0.7013 ± 0.0391 | 2.6435 ± 0.2494 |
| 5 | acetic acid | 7.958 | 0.017 ± 0.0035 | 0.0155 ± 0.0037 | 0.0168 ± 0.0047 | 0.0164 ± 0.0043 | 0.0142 ± 0.0041 | 0.013 ± 0.0032 |
| 6 | dimethyl tartarate | 8.001 | 0.0158 ± 0.0016 | 0.0184 ± 0.0022 | 0.0181 ± 0.0036 | 0.0194 ± 0.0042 | 0.0214 ± 0.006 | 0.0195 ± 0.0039 |
| 7 | 3-hydroxybutyric acid | 8.148 | 0.1576 ± 0.0461 | 0.2662 ± 0.0734 | 0.21 ± 0.0538 | 0.1243 ± 0.0372 | 0.205 ± 0.0589 | 0.1964 ± 0.0395 |
| 8 | L-valine | 9.143 | 0.2752 ± 0.0775 | 0.5701 ± 0.0699 | 0.7405 ± 0.0437 | 0.2561 ± 0.0731 | 0.6827 ± 0.0626 | 0.3354 ± 0.0146 |
| 9 | L-asparagine | 9.199 | 0.0234 ± 0.0031 | 0.0192 ± 0.0029 | 0.025 ± 0.0064 | 0.0235 ± 0.0047 | 0.0241 ± 0.0055 | 0.0228 ± 0.003 |
| 10 | urea | 9.745 | 3.4151 ± 0.6285 | 3.5867 ± 0.7607 | 4.2767 ± 1.1888 | 3.6721 ± 0.6969 | 4.1347 ± 1.0551 | 3.8493 ± 0.5092 |
| 11 | L-leucine | 10.164 | 0.153 ± 0.0159 | 0.2016 ± 0.0203 | 0.2098 ± 0.045 | 0.1707 ± 0.0278 | 0.1817 ± 0.0323 | 0.1848 ± 0.0281 |
| 12 | phosphate | 10.297 | 3.3269 ± 0.2384 | 3.4245 ± 0.3453 | 3.4822 ± 0.2747 | 2.4444 ± 0.2075 | 2.3336 ± 0.2735 | 2.9413 ± 0.3261 |
| 13 | L-proline | 10.565 | 0.3774 ± 0.0827 | 0.3286 ± 0.0284 | 0.4078 ± 0.0941 | 0.3752 ± 0.1099 | 0.4422 ± 0.0987 | 0.4122 ± 0.0621 |
| 14 | glycine | 10.745 | 0.1442 ± 0.0401 | 0.2752 ± 0.0667 | 0.2418 ± 0.0643 | 0.1558 ± 0.0751 | 0.2747 ± 0.0633 | 0.1817 ± 0.0509 |
| 15 | butanedioic acid | 10.819 | 0.0292 ± 0.0058 | 0.0334 ± 0.0078 | 0.0272 ± 0.0016 | 0.0263 ± 0.0047 | 0.0375 ± 0.0035 | 0.0314 ± 0.0049 |
| 16 | glyceric acid | 11.237 | 0.0239 ± 0.0071 | 0.0215 ± 0.0065 | 0.0204 ± 0.0009 | 0.0262 ± 0.0058 | 0.0207 ± 0.006 | 0.0203 ± 0.0021 |
| 17 | serine | 11.756 | 0.362 ± 0.0516 | 0.4009 ± 0.0606 | 0.4694 ± 0.0936 | 0.3591 ± 0.0792 | 0.3508 ± 0.0531 | 0.3296 ± 0.0417 |
| 18 | L-threonine | 12.25 | 0.3899 ± 0.0337 | 0.3833 ± 0.0353 | 0.3567 ± 0.089 | 0.3662 ± 0.0656 | 0.3743 ± 0.0684 | 0.3846 ± 0.0863 |
| 19 | aminomalonic acid | 13.764 | 0.0703 ± 0.0141 | 0.0635 ± 0.0175 | 0.0659 ± 0.0162 | 0.0454 ± 0.0135 | 0.0548 ± 0.0142 | 0.0583 ± 0.0111 |
| 20 | malic acid | 14.14 | 0.0258 ± 0.0038 | 0.0281 ± 0.0039 | 0.0253 ± 0.0018 | 0.0237 ± 0.0036 | 0.029 ± 0.003 | 0.0386 ± 0.0105 |
| 21 | pyroglutamic acid | 14.674 | 0.6946 ± 0.0526 | 0.8060 ± 0.0626 | 0.7210 ± 0.0561 | 0.6826 ± 0.0312 | 0.7739 ± 0.0639 | 0.6023 ± 0.034 |
| 22 | 4-hydroxyproline | 14.844 | 0.1202 ± 0.0135 | 0.1000 ± 0.0215 | 0.1065 ± 0.0280 | 0.0876 ± 0.0175 | 0.0932 ± 0.0098 | 0.0919 ± 0.0258 |
| 23 | L-ornithine | 16.56 | 0.0745 ± 0.0216 | 0.0556 ± 0.0141 | 0.0729 ± 0.0211 | 0.0508 ± 0.0132 | 0.0498 ± 0.014 | 0.0568 ± 0.0168 |
| 24 | L-glutamic acid | 16.683 | 0.1114 ± 0.024 | 0.1257 ± 0.0071 | 0.1089 ± 0.0282 | 0.0586 ± 0.0093 | 0.0755 ± 0.0139 | 0.0936 ± 0.0215 |
| 25 | phenylalanine | 16.725 | 0.0725 ± 0.0127 | 0.0906 ± 0.0243 | 0.0873 ± 0.0142 | 0.0773 ± 0.0142 | 0.0803 ± 0.0162 | 0.0817 ± 0.0074 |
| 26 | asparagine | 17.715 | 0.0598 ± 0.0173 | 0.0402 ± 0.0099 | 0.044 ± 0.0055 | 0.0393 ± 0.0104 | 0.0482 ± 0.0123 | 0.0411 ± 0.0093 |
| 27 | L-(−)-sorbose | 18.149 | 0.0297 ± 0.0039 | 0.0325 ± 0.0089 | 0.0388 ± 0.0084 | 0.0268 ± 0.0079 | 0.0292 ± 0.0047 | 0.0344 ± 0.0041 |
| 28 | L-glutamine | 19.723 | 0.2525 ± 0.0097 | 0.2254 ± 0.067 | 0.2264 ± 0.0458 | 0.101 ± 0.0386 | 0.1063 ± 0.0574 | 0.147 ± 0.0177 |
| 29 | citric acid | 20.824 | 0.3993 ± 0.0656 | 0.2353 ± 0.0988 | 0.2717 ± 0.0703 | 0.3506 ± 0.0396 | 0.2593 ± 0.0678 | 0.3063 ± 0.0477 |
| 30 | 1,5-anhydrohexitol | 21.413 | 0.2521 ± 0.0493 | 0.2678 ± 0.0647 | 0.2785 ± 0.0647 | 0.2193 ± 0.0238 | 0.1956 ± 0.0285 | 0.2159 ± 0.056 |
| 31 | D-(−)-fructose | 22.058 | 0.4894 ± 0.0961 | 0.2798 ± 0.0759 | 0.548 ± 0.1283 | 0.3206 ± 0.0679 | 0.161 ± 0.0259 | 0.2323 ± 0.0478 |
| 32 | D-mannose | 22.35 | 1.3469 ± 0.0344 | 0.6741 ± 0.0775 | 0.7757 ± 0.0314 | 1.2705 ± 0.0886 | 0.6054 ± 0.0244 | 0.9205 ± 0.0411 |
| 33 | D-glucose | 22.630; 22.91 | 20.2195 ± 1.4848 | 21.1729 ± 1.0042 | 23.1447 ± 0.9519 | 17.1469 ± 1.432 | 17.5381 ± 1.6458 | 21.4798 ± 0.6572 |
| 34 | maltose | 23.549; 24.117 | 2.2709 ± 0.1667 | 1.1877 ± 0.0617 | 1.1043 ± 0.0744 | 2.2114 ± 0.1041 | 0.5867 ± 0.078 | 1.1246 ± 0.1023 |
| 35 | palmitic acid | 24.598 | 0.3299 ± 0.0598 | 0.3822 ± 0.0588 | 0.3281 ± 0.0448 | 0.2925 ± 0.0305 | 0.3244 ± 0.0531 | 0.2987 ± 0.0347 |
| 36 | D-galactose | 25.019 | 0.1213 ± 0.0272 | 0.0779 ± 0.0125 | 0.7583 ± 0.0454 | 0.1131 ± 0.0341 | 0.0949 ± 0.0327 | 0.1295 ± 0.046 |
| 37 | myo-inositol | 25.994 | 0.2774 ± 0.0794 | 0.2342 ± 0.0315 | 0.2774 ± 0.0375 | 0.2142 ± 0.0271 | 0.2315 ± 0.0687 | 0.2097 ± 0.0369 |
| 38 | D-glucopyranosiduronic acid | 26.169 | 0.0375 ± 0.0059 | 0.0529 ± 0.0157 | 0.0334 ± 0.0096 | 0.028 ± 0.0079 | 0.0274 ± 0.0021 | 0.0306 ± 0.0054 |
| 39 | linoleic acid | 27.509 | 0.1497 ± 0.0279 | 0.1935 ± 0.0374 | 0.1827 ± 0.0532 | 0.1179 ± 0.0148 | 0.0875 ± 0.0171 | 0.1345 ± 0.0248 |
| 40 | 9-octadecenoic acid | 27.599 | 0.0658 ± 0.0085 | 0.0951 ± 0.0265 | 0.0957 ± 0.023 | 0.0552 ± 0.009 | 0.0425 ± 0.0124 | 0.0776 ± 0.0116 |
| 41 | L-tryptophan | 27.916 | 0.0913 ± 0.0099 | 0.0968 ± 0.0268 | 0.1333 ± 0.0212 | 0.0711 ± 0.0057 | 0.0942 ± 0.0249 | 0.0729 ± 0.0124 |
| 42 | stearic acid | 28.053 | 0.2207 ± 0.0171 | 0.2768 ± 0.0326 | 0.2376 ± 0.035 | 0.1993 ± 0.0203 | 0.2341 ± 0.0395 | 0.2151 ± 0.0321 |



https://doi.org/10.1021/acsomega.1c02370
ACS Omega 2021, 6, 19717−19730

Table 1. continued

| peak no. | metabolite | $R_t$ (min) | 1 day | | | 7 days | | |
|---|---|---|---|---|---|---|---|---|
| | | | control | PQ | XBJ | control | PQ | XBJ |
| 43 | D-galacturonic acid | 29.43 | 0.1927 ± 0.0515 | 0.0928 ± 0.004 | 0.0859 ± 0.0569 | 0.2221 ± 0.0801 | 0.0931 ± 0.0785 | 0.2358 ± 0.0943 |
| 44 | edetic acid | 30.116 | 0.0715 ± 0.0107 | 0.071 ± 0.0163 | 0.0636 ± 0.0047 | 0.0409 ± 0.0108 | 0.0358 ± 0.0104 | 0.0366 ± 0.0095 |
| 45 | arachidonic acid (AA) | 31.519 | 5.5582 ± 0.5835 | 8.075 ± 0.4736 | 6.3639 ± 0.3627 | 5.2254 ± 0.5695 | 8.0458 ± 0.4815 | 7.4974 ± 0.4512 |
| 46 | cholesterol | 34.551 | 0.5281 ± 0.0733 | 0.6722 ± 0.0818 | 0.6622 ± 0.064 | 0.4062 ± 0.053 | 0.4423 ± 0.0947 | 0.5582 ± 0.0217 |

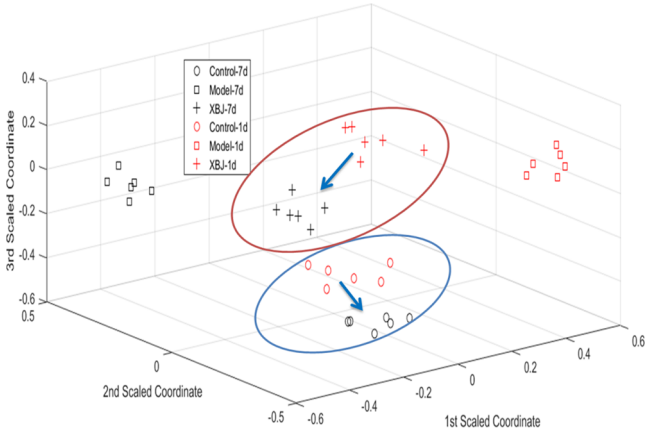


**Figure 4.** Classification plots of different groups.

was downloaded according to the set conditions, and the downloaded TSV format file was put into Cytoscape 3.7.0 software for network analysis and core target gene screening (Figure 9 and Table 3). The PPI analysis revealed that JUN had the largest degree value, followed by TP53, MYC, and MAPK14. The results showed that XBJ had the characteristics of multicomponent and multitarget action in the treatment of pulmonary fibrosis.

Gene ontology (GO) functional enrichment analysis showed that a total of 2821 items were enriched ($P < 0.05$), including 2512 items of the biological process (BP), 95 items in the cell composition (CC), and 213 items of molecular function (MF). The top 10 major biological processes were arranged by $P$ values from small to large (Figure 10). Rich targets mainly involved the cellular response to chemical stress, response to oxidative stress, response to metal ions, membrane raft, membrane microdomain, membrane region, nuclear receptor activity, ligand-activated transcription factor activity, nuclear receptor activity, steroid hormone receptor activity, and other biological processes.

KEGG signaling pathway analysis obtained a total of 167 signaling pathways, and the top 20 major signaling pathways were selected by ranking the $P$-value from small to large ($P < 0.05$). The selected pathways mainly included fluid shear stress and atherosclerosis, the age-range signaling pathway in diabetic complications, hepatitis B, and prostate cancer; interleukin 17 (IL-17)-signaling pathway in small-cell lung cancer; and the tumor necrosis factor (TNF) signaling pathway, among other pathways (Figure 11).

**2.6. Joint Pathway Analysis.** The combined pathway analysis was performed with 180 targets obtained from network pharmacology and 8 differential metabolites obtained from plasma metabolomics. The obtained results are shown in Figure 12A. The arachidonic acid pathway is a common signaling pathway in network pharmacology and metabolomics. It has been reported that the arachidonic acid signaling pathway is mainly used for the synthesis of inflammatory mediators. It can mediate the production of a variety of inflammatory factors, such as monocyte chemotactic protein 1 (MCP-1), tumor necrosis factor (TNF), IL, interferon (IFN), etc., and it is closely related to the occurrence, development, and regression of inflammation.[22] The enrichment analysis results of the KEGG signaling pathway are shown in Figure 11. The TNF signaling pathway is highly enriched and is one of


https://doi.org/10.1021/acsomega.1c02370
ACS Omega 2021, 6, 19717−19730

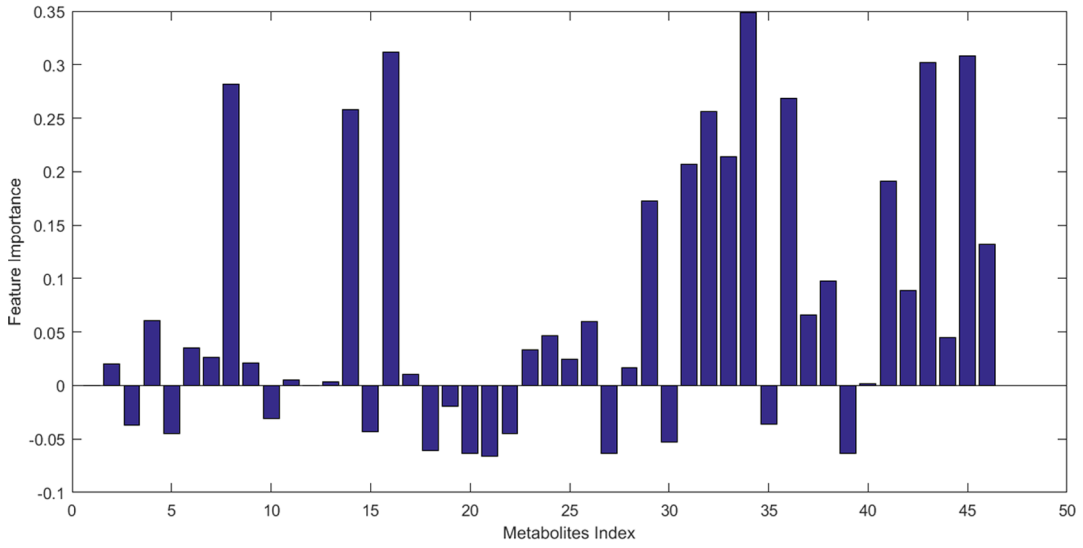


**Figure 5.** VIP value of each metabolite to discriminate between PQ poisoning and healthy control groups.

**Table 2. Statistical Analysis of Differential Metabolites for 7 days**[a]

| metabolite | control:PQ | PQ:XBJ | control:XBJ | pathway analysis |
|---|---|---|---|---|
| L-valine | ↑** | ↓* | / | valine, leucine, and isoleucine biosynthesis |
| glycine | ↑** | ↓* | / | glycine, serine, and threonine metabolism |
| citric acid | ↑** | ↓* | ↓* | starch and sucrose metabolism |
| D-mannose | ↓** | ↑** | ↓* | fructose and mannose metabolism |
| D-galactose | ↓** | ↑** | / | starch and sucrose metabolism |
| L-tryptophan | ↑* | ↓* | / | tryptophan metabolism |
| arachidonic acid | ↑** | ↓** | / | arachidonic acid metabolism |

[a]↑ Metabolites were upregulated; ↓ metabolites were downregulated; and *$P$ < 0.05, **$P$ < 0.01, and / represents $P$ > 0.05.

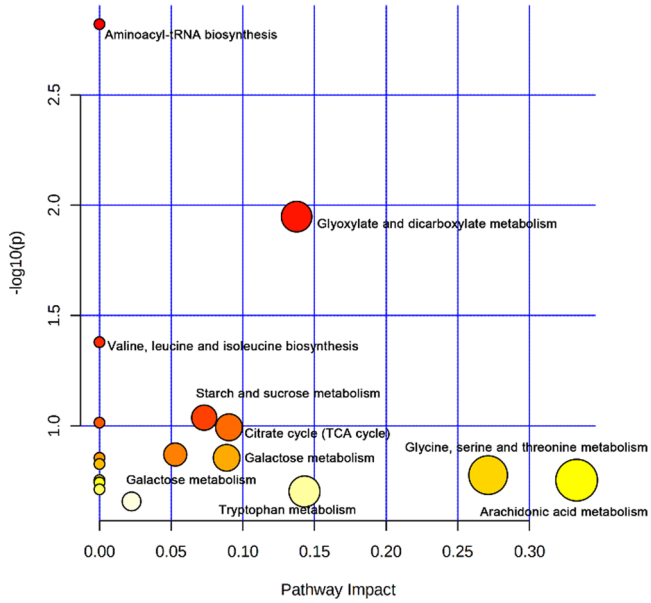


**Figure 6.** Summary of metabolic pathway analysis.

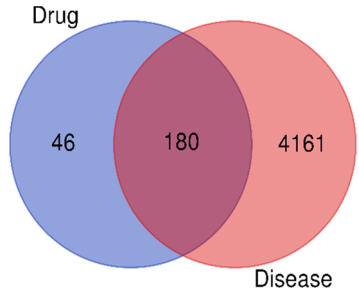


**Figure 7.** Intersection of drug targets and disease targets. The drug represents XBJ, and the disease represents pulmonary fibrosis. The intersection section represents the common target.

the key signaling pathways. The targets involved in the TNF signaling pathway include p65, IKB$\alpha$, and IKK$\beta$ (Figure 12B).

**2.7. Molecular Docking.** Based on the metabolomics and network pharmacology findings, we focused on the molecular docking of target proteins in their common pathways with their corresponding active components. It is generally believed that the more stable the conformation of the active compound binding to the protein receptor, the lower the energy and the greater the possibility of interaction. Here, the composition with a binding energy ≤−5 kJ/mol (about −1.2 kcal/mol) was selected as the evaluation standard. Molecular docking results showed that the binding energies of AKT1, FOS, MAPK1, MAPK8, MAPK14, and TNF with the ligand of the corresponding active compounds was far less than −5 kJ/mol (Table 4 and Figure 13), indicating that the compounds had strong binding activity with the target protein and were important active compounds of XBJ against pulmonary fibrosis.

**2.8. XBJ Alleviates Pulmonary Fibrosis by Inhibiting Inflammation.** To determine whether inflammation is involved in the XBJ effect, resistance to pulmonary fibrosis was assessed by western blot of TNF signaling pathway members p-p65, p-IKB$\alpha$, and p-IKK$\beta$. Results show that PQ-treated RAW 264.7 cells had signficantly higher expressions of p-p65, p-IKB$\alpha$, and p-IKK$\beta$ compared with both the blank group and the PQ + XBJ group ($P$ < 0.05). There were no significant differences in the protein expression between the


https://doi.org/10.1021/acsomega.1c02370
ACS Omega 2021, 6, 19717−19730

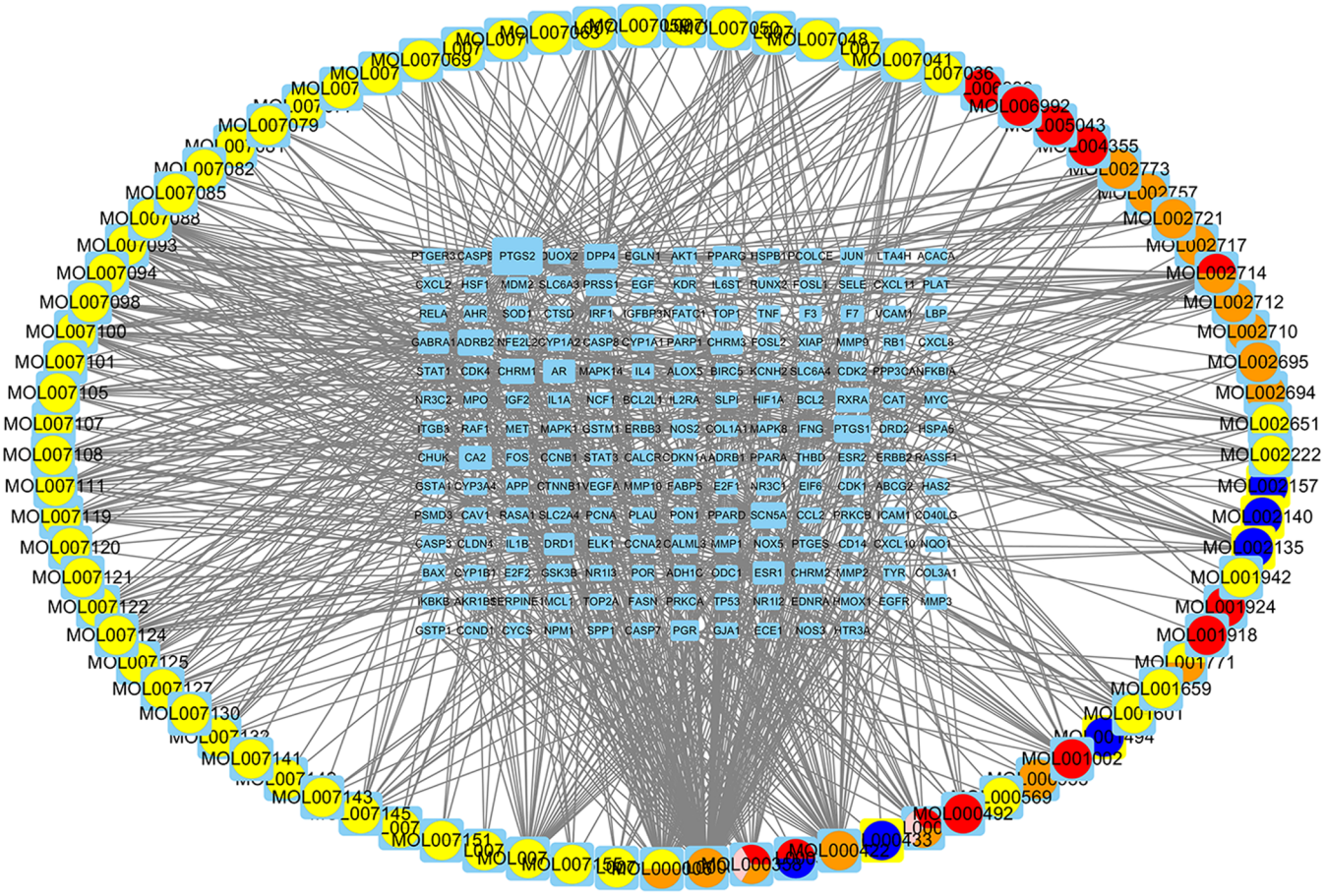

**Figure 8.** Active ingredient−target−disease network diagram. Yellow represents *S. miltiorrhiza*, red represents *P. lactiflora*, blue represents ligusticum chuanxiong, pink represents *A. sinensis*, and orange represents *C. tinctorius and* the line represents the relationship between the drug, the disease, and the target of action.

XBJ and blank groups (Figure 14). Above all, XBJ injection can inhibit the inflammatory response to suppress the development of pulmonary fibrosis induced by PQ.

## 3. DISCUSSION

Eight potential biomarkers of PQ poisoning were identified: L-valine, glycine, citric acid, D-mannose, D-galactose, maltose, L-tryptophan, and arachidonic acid. L-Valine is an essential amino acid that promotes growth, repairs tissues, and regulates blood sugar. During intense physical activity, L-valine can provide extra energy for muscles by producing glucose and remove excess nitrogen (a potential toxin) from the liver.[23] As a nonessential amino acid and intermediate of threonine and serine metabolism, glycine has an important antioxidant effect.[24] Glycine can reduce protein carbonylation and lipid peroxidation by decreasing the release of superoxide free radicals. Tryptophan is an essential aromatic amino acid. An excess of L-tryptophan can cause hypoxemia, peripheral eosinophilia, dyspnea, fatigue, and weakness, which are similar to the symptoms of PQ poisoning.[25] In vivo, L-tryptophan can produce indole sulfate, which reduces glutathione levels[26] and regulates the response to oxidative stress.[27] It is generally believed that lung injury caused by PQ poisoning is mainly related to reduction of active oxygen, lipid hydroperoxides, and the glutathione concentration. Superoxide free radicals, lipid peroxides, and other reactive oxygen species (ROS) are associated with the occurrence and development of pulmonary fibrosis.[28] In this study, the levels of L-valine, glycine, and L-tryptophan in the PQ poisoning group increased significantly compared with those in the control group. After treatment with XBJ injection, the relative levels of the three amino acid metabolites were reversed, indicating that XBJ could inhibit PQ poisoning by regulating amino acid metabolism.

PQ can induce redox reactions and interfere with mitochondrial electron transfer to produce a large number of oxygen free radicals. Mitochondria are important in the tricarboxylic acid (TCA) cycle,[29] of which citric acid is an intermediate.[30] In our study, the level of citric acid increased significantly in the PQ group, indicating that the TCA cycle was blocked and the energy supply was affected. After XBJ treatment, the content of citric acid decreased significantly. Therefore, XBJ can reverse the effects of PQ toxicity by improving the function of the TCA cycle to regulate energy metabolism.

D-Mannose, D-galactose, and maltose are products of glucose metabolism. They provide energy through the pentose phosphate pathway and glycolysis. D-Mannose is a substrate of the glycolysis pathway and has important roles in glycosylation of many proteins and in the immune system.[31,32] In a previous study, the concentrations of D-mannose and D-galactose in human bronchial epithelial cells from patients with cystic fibrosis were greatly reduced because of glucose metabolism inhibition.[33,34] Our research showed that levels of D-mannose, D-galactose, and maltose were low in the PQ


https://doi.org/10.1021/acsomega.1c02370
ACS Omega 2021, 6, 19717−19730

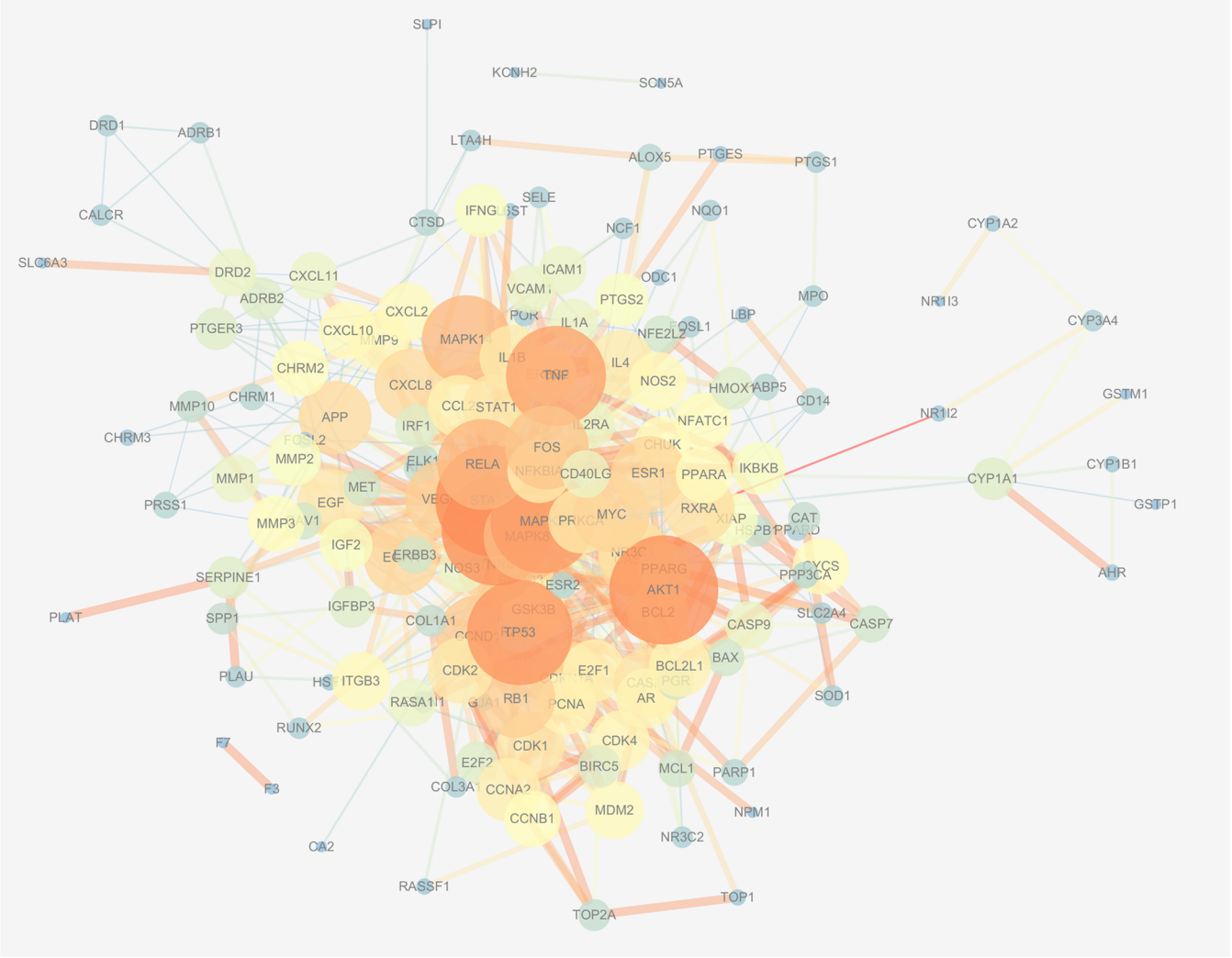


**Figure 9.** XBJ antipulmonary fibrosis PPI network of 156 nodes and 737 edges. (The darker the red, the higher the degree of connection).

**Table 3. Degree of the Antipulmonary Fibrosis Core Target of XBJ**

| target's name | betweenness | closeness | degree |
|---|---|---|---|
| JUN | 12.76991 | 1 | 15 |
| TP53 | 7.315152 | 0.882353 | 13 |
| MYC | 6.291342 | 0.833333 | 12 |
| MAPK14 | 7.86746 | 0.833333 | 12 |
| FOS | 4.324675 | 0.833333 | 12 |
| STAT3 | 4.523882 | 0.789474 | 11 |
| MAPK1 | 5.748413 | 0.789474 | 11 |
| MAPK8 | 5.249278 | 0.789474 | 11 |
| CCND1 | 4.593651 | 0.75 | 10 |
| ESR1 | 2.697691 | 0.75 | 10 |
| AKT1 | 2.658009 | 0.75 | 10 |
| NR3C1 | 1.58658 | 0.714286 | 9 |
| RELA | 2.447691 | 0.714286 | 9 |
| CDKN1A | 1.742857 | 0.681818 | 8 |
| TNF | 0.985714 | 0.681818 | 8 |
| RB1 | 1.197691 | 0.652174 | 7 |

poisoning group and that XBJ reduced PQ-induced energy metabolism dysfunction by regulating glucose metabolism.

Arachidonic acid (AA) is an unsaturated fatty acid catalyzed by phospholipase A2 (PLA2). AA can produce a variety of metabolites through cyclooxygenase (COX), lipoxygenase (LOX), and cytochrome P450 (CYP450) pathways. It is also widely involved in inflammation, immune regulation, cellular immunity, and other important reactions. COX inhibitors inhibit the expression of inflammatory factors such as IL-6, TNF-$\alpha$, IFN-$\alpha$, and IFN-$\beta$. LOX can stimulate the production of inflammatory cytokines such as IL-6, IL-12, TNF-$\alpha$, and MCP-1, which participate in a variety of inflammatory response processes and promote white blood cell migration, resulting in multiple organ failure.[3,34−36] We found that the level of arachidonic acid increased in the PQ poisoning group. Arachidonic acid serves as a biomarker that indicates ROS activation and release in the body following PQ. By regulating fatty acid metabolism, it can reduce ROS release and inflammatory factors and reduce the pulmonary inflammatory response.

Network pharmacology is a discipline based on systems biology and pharmacology. It reflects the characteristics of interactions among multiple components, multiple targets, multiple pathways, and complex diseases of traditional Chinese medicine. Molecular docking is a commonly used method to identify the interaction between receptor proteins and molecules with high accuracy.[37] Based on the metabolomics results, combined with the predictions from network


https://doi.org/10.1021/acsomega.1c02370
ACS Omega 2021, 6, 19717−19730

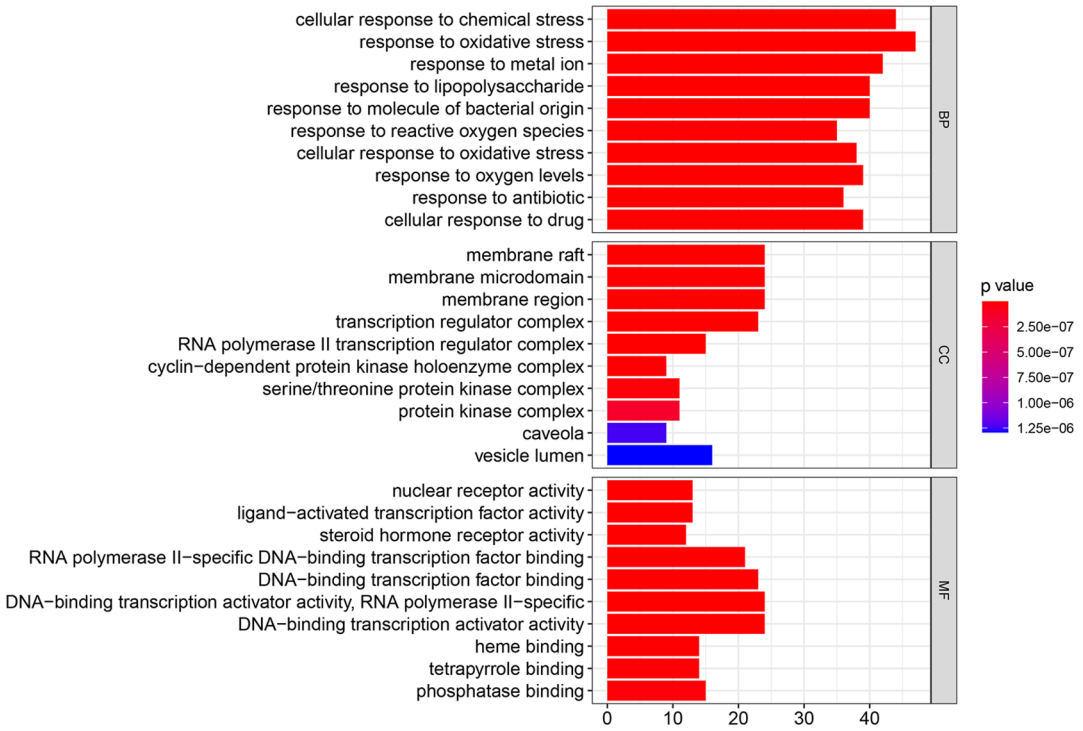


**Figure 10.** GO functional enrichment analysis diagram. The top 20 GO functional items with $P < 0.05$ were chosen.

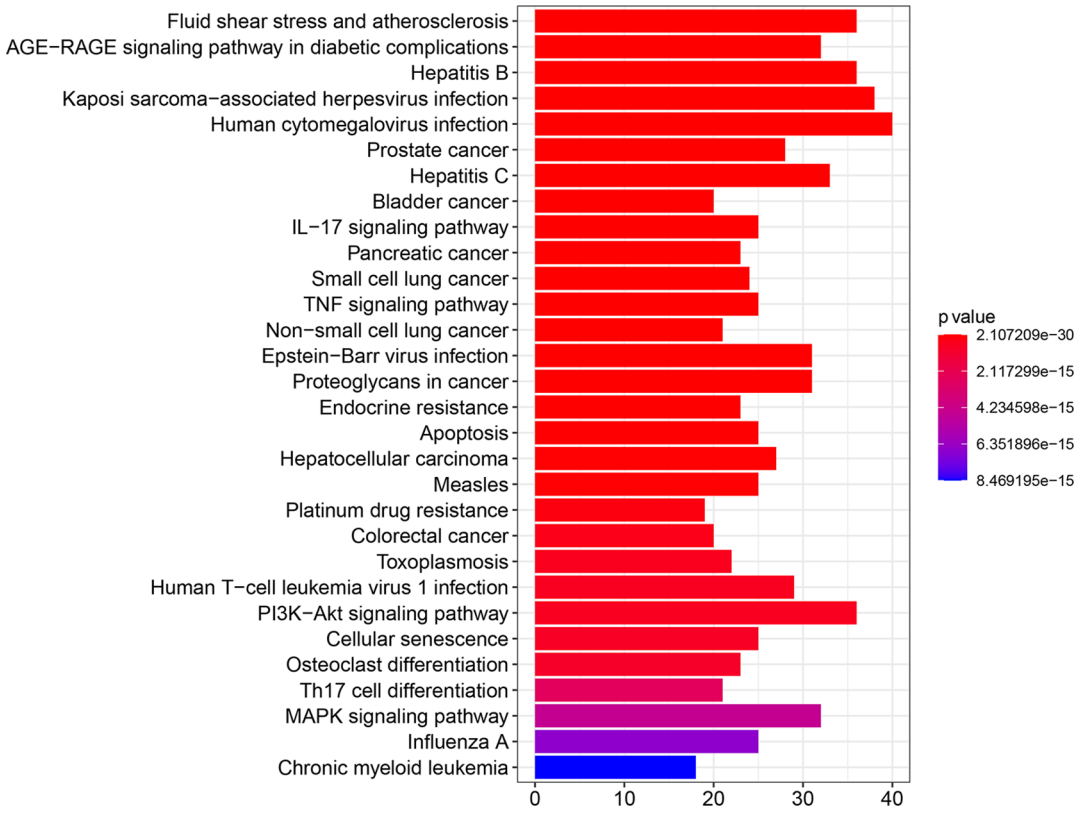


**Figure 11.** Enrichment analysis of the KEGG signaling pathway. Pathways that had great changes of $P < 0.05$ were chosen.

pharmacology and molecular docking analyses, 125 XBJ active components and 180 related targets for the treatment of pulmonary fibrosis were found in this study. Molecular docking analysis showed that the binding energy between the core target and the corresponding active compound ligand of XBJ was much lower than −5 kJ/mol, indicating strong binding activity. Therefore, the active components of XBJ injection against PQ-induced pulmonary fibrosis are mainly baicalein, $\beta$-carotene, kaempferol, luteolin, quercetin, tanshinone IIA, and myrcene ketone. The arachidonic acid metabolic pathway is


https://doi.org/10.1021/acsomega.1c02370
ACS Omega 2021, 6, 19717−19730

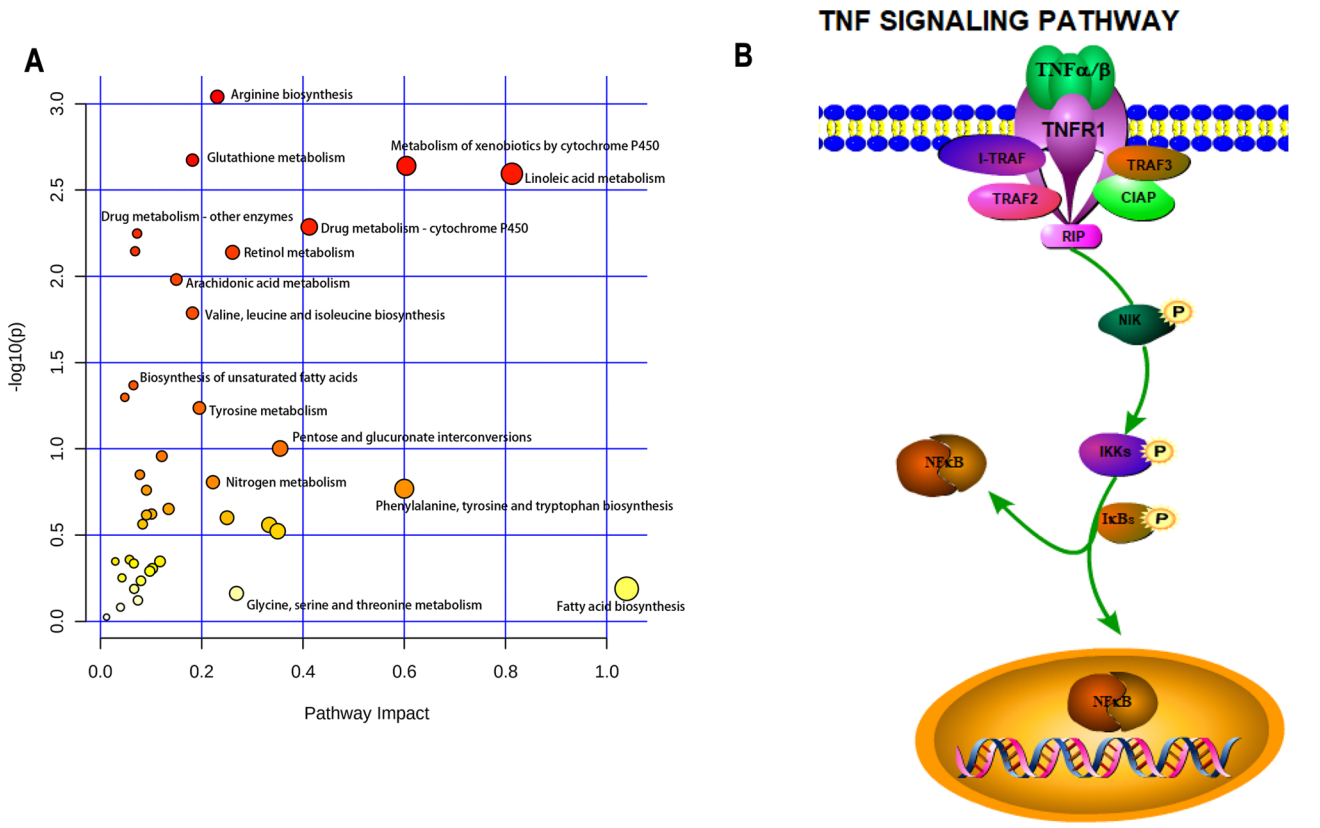


**Figure 12.** (A) Network pharmacology and the metabonomics combined analysis pathway diagram. (B) TNF signaling pathway.

**Table 4. Docking Effect Analysis of Compounds and Targets**

| compound | target | PDB ID | binding energy (kcal/mol) |
|---|---|---|---|
| baicalein | AKT1 | 5WBL | −6.2 |
| | FOS | 1FOS | −9.3 |
| *β*-carotene | AKT1 | 5WBL | −6.8 |
| kaempferol | AKT1 | 5WBL | −6.3 |
| | MAPK8 | 3ELJ | −5.7 |
| | TNF | 2ZPX | −7.7 |
| luteolin | AKT1 | 5WBL | −6.7 |
| | MAPK1 | 4FV5 | −8.9 |
| | TNF | 2ZPX | −8.6 |
| quercetin | AKT1 | 5WBL | −7.0 |
| | FOS | 1FOS | −10.4 |
| | MAPK1 | 4FV5 | −8.9 |
| | TNF | 2ZPX | −8.8 |
| tanshinone IIA | FOS | 1FOS | −8.6 |
| | MAPK14 | 4GEO | −7.8 |
| myricanone | MAPK14 | 4GEO | −7.4 |

mainly used for the synthesis of inflammatory mediators, such as TNF. In the TNF signaling pathway, TNF-*α* acts as an agonist to further enhance the transcriptional activity of the nuclear factor (NF)-*κ*B and stimulate the activation of NF-*κ*B. Activation of NF-*κ*B enhances the transcription of TNF-*α* and IL-1*β* and thus increases the production and release of TNF-*α* and IL-1*β*. The newly produced TNF-*α* and IL-1*β* then reactivate NF-*κ*B and increase the production and release of proinflammatory cytokines such as IL-6 and IL-8. Therefore, the activated NF-*κ*B, in turn, increases the formation of TNF-*α*, and the positive feedback regulatory loop formed by the two can continuously expand the inflammatory response and deepen the degree of fibrosis.[38,39] Combined analysis of network pharmacological targets and metabolites based on metabolic analysis techniques revealed that inhibition of the arachidonic acid metabolism pathway and downstream TNF signaling pathway can inhibit the production of a variety of inflammatory factors, thereby reducing the degree of pulmonary fibrosis. In this study, the western blot analysis further confirmed that XBJ injection can alleviate pulmonary fibrosis by inhibiting the TNF signaling pathway. The results showed that XBJ could decrease the expression of p-p65, p-IKB*α*, and p-IKK*β*, which confirmed that XBJ injection could inhibit the inflammatory response and thus inhibit the development of pulmonary fibrosis induced by paraquat.

## 4. CONCLUSIONS

In this study, a GC−MS-based metabolic assay and network pharmacological analysis were established to explore the mechanism of paraquat-induced pulmonary fibrosis and reveal the molecular mechanism of XBJ injection in the treatment of pulmonary fibrosis. Metabonomics analysis showed that three types of metabolites, i.e., amino acids, saccharides, and free acids, showed higher contributions in distinguishing the PQ group and control group. Levels of these metabolites were correlated with amino acid metabolism, energy metabolism, and free acid metabolism. The network pharmacological analysis showed that XBJ injection could exert antipulmonary fibrosis effects through multiple targets, multiple components, multiple signal pathways, and multiple metabolic pathways. Combined pathway analysis showed that arachidonic acid metabolism was the most important metabolic pathway. Additionally, the western blot analysis confirmed that XBJ injection could alleviate the development of pulmonary fibrosis


https://doi.org/10.1021/acsomega.1c02370
ACS Omega 2021, 6, 19717−19730

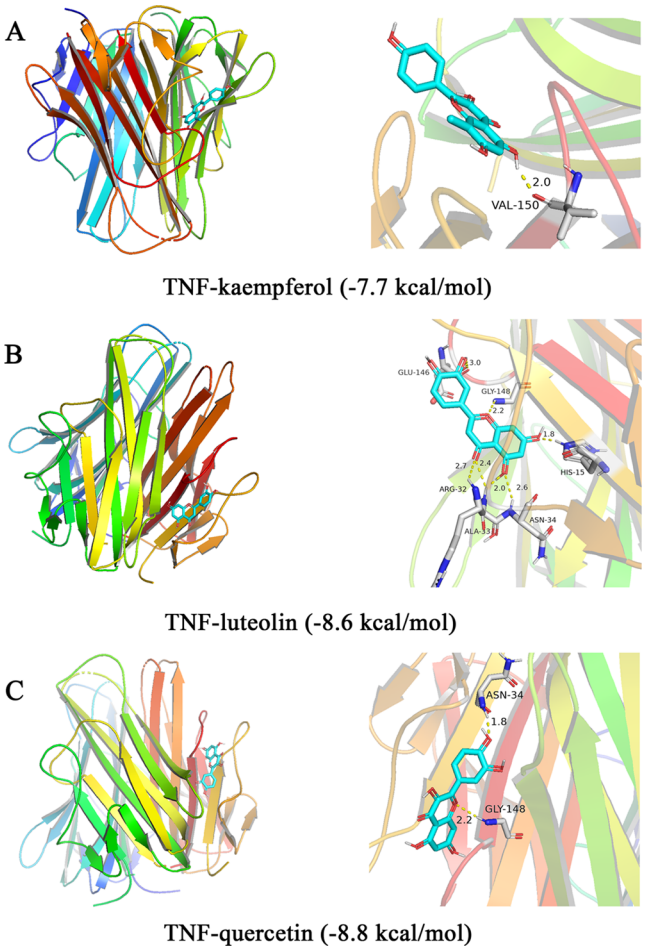


**Figure 13.** Result of molecular docking. (A) TNF-kaempferol, (B) TNF-luteolin, and (C) TNF-quercetin. A blue object represents a compound and the surrounding chain represents an anti-inflammatory target.

by inhibiting inflammation. The results showed that XBJ injection could regulate the metabolism of amino acids, fatty acids, and energy, and inhibit the inflammatory response to treat pulmonary fibrosis induced by paraquat.

## 5. MATERIALS AND METHODS

**5.1. Equipment, Chemicals, and Reagents.** Sample analysis was performed with GC−MS (7890A-5975C, Agilent, Santa Clara, CA) using ChemStation software (Agilent) and the NIST mass spectral library. A high-speed centrifuge (5415R, Eppendorf Centrifuge, Germany), vortex mixer (MX-F, Scilogex), DYY-7C electrophoresis apparatus, electrophoresis tank, transfer printing tank, and Chemidoc MP gel imaging system (Bio-RAD) were used in the experiments.

Xuebijing (XBJ) injection, prepared from extracts of *C. tinctorius*, *P. lactiflora* roots, ligusticum chuanxiong rhizomes, *A. sinensis* roots, and *S. miltiorrhiza* roots was provided by Tianjin Chase Sun Pharmaceutical Co., Ltd. (Tianjin, China; lot 2006241). PQ was purchased from Shenzhen Nantong Crop Protection Priority Company (Shenzhen, China). Methanol and 2-isopropylmalic acid for chromatography were purchased from Sigma-Aldrich (St. Louis, MO). *N*,*O*-Bis(trimethylsilyl)-trifluoroacetamide containing 1% trimethylchlorosilane was purchased from AccuStandard (New Haven, CT). Methoxyamine hydrochloride, pyridine, hydrazine, oxalic acid, palmitic acid, glucose, and cholesterol were purchased from Sigma-Aldrich. RAW264.7 cells, p65 (8242S), IKB$\alpha$ (4814S), IKK$\beta$ (8943S), p-p65 (3033S), p-IKB$\alpha$ (2859S), and p-IKK$\beta$ (8943S) were purchased from Cell Signaling Technology.

**5.2. Animal Models.** Thirty-six male Sprague Dawley rats weighing 210 ± 10 g were obtained from Hunan Silaike Jingda Laboratory Animal Co. (Changsha, China). The animal license number was SCXK (Xiang) 2019-0004 (approved by the Hunan Provincial Science and Technology Department, China). The experiment was approved by the Medical Ethics Committee of Hunan Provincial People's Hospital (lot no. 202105). All rats were housed at the Animal Research Center of Hunan Provincial People's Hospital under controlled conditions at a temperature of 22 °C and a natural light−dark cycle.

Rats were randomly divided into PQ-poisoning, XBJ-treatment, and control groups ($n$ = 12 in each group). Each group was further divided into two subgroups, with one subgroup treated for 1 day and the other treated for 7 days ($n$ = 6 in each subgroup). The PQ and XBJ groups were intragastrically administered 40 mg/kg PQ. The control group was administered 1 mL of normal saline. The XBJ group had a further intraperitoneal injection of 8 mL/(kg days) XBJ after intragastric administration of PQ for 2 h. In place of XBJ, the PQ and control groups received an intraperitoneal injection of the same volume of normal saline. Activity of the rats was observed daily. All experimental procedures were conducted according to the Guidelines of Animal Care and received ethical approval from the Administration Committee of Experimental Animals of the Animal Research Center of Hunan Provincial People's Hospital.

**5.3. Serum Collection and Preparation.** After the last treatment dose for each group, all rats were anesthetized with

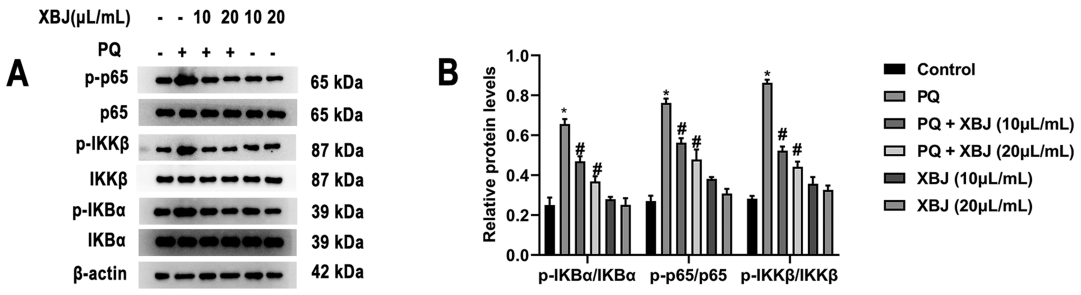


**Figure 14.** (A) Effect of XBJ on expression of inflammatory pathway-related proteins in PQ-induced RAW 264.7 cells. (B) Histograms show the relative expression of each group. Data are represented as mean ± SD ($n$ = 3), * represents the comparison between PQ and the control groups, * represents $P < 0.05$, # represents the comparison between XBJ + PQ and PQ groups, and # represents $P < 0.05$.



https://doi.org/10.1021/acsomega.1c02370
ACS Omega 2021, 6, 19717−19730

10% chloral hydrate. Blood samples were collected from the heart and centrifuged at 16 000 rpm/min. About 200 μL of the supernatant was then transferred to a 1.5 mL centrifuge tube and stored at −80 °C until required for analysis.

Lung tissues were removed by thoracotomy, and the right lower lobe tissue was immersed in 10% neutral formaldehyde for 48 h, embedded in paraffin, and trisected. Hematoxylin−eosin staining was performed using a standard protocol,[40] and lung tissue pathological changes were observed under a light microscope. The remaining lung tissue was frozen in liquid nitrogen in a 1.5 mL Eppendorf tube and stored at −80 °C until required for analysis.

The sample preparation process was optimized according to previously reported methods.[41] A 200 μL aliquot of each serum sample was thawed at 4 °C and mixed with 50 μL of 2-isopropylmalic acid (1.1 mg/mL) as an internal standard by vortexing for 20 s. After addition of 600 μL of methanol, the sample was vortexed for 20 s and centrifuged at 16 000 rpm/min for 15 min to remove the protein. Subsequently, the supernatant was placed in a glass centrifuge tube and dried under a stream of nitrogen gas at room temperature. The residue was dissolved in 100 μL of methoxyamine solution (20 mg/mL in pyridine), vortexed for 45 s, and incubated at 70 °C for 1 h. A quantity of 100 μL of *N*,*O*-bis(trimethylsilyl)-trifluoroacetamide containing 1% trimethylchlorosilane was then added to the sample, followed by vortexing for 15 s and incubating for 1 h at 70 °C to increase the volatility of the metabolite. Finally, 100 μL of the cooled sample was used for GC−MS analysis.

**5.4. GC−MS Analysis.** The samples were separated on a fused silica capillary column (HP-5MS, 30 m × 0.25 mm i.d., 0.25 μm, Agilent) using the following temperature program: 80 °C for 2 min, increased to 240 °C at a rate of 4 °C/min, increased to 280 °C at a rate of 10 °C/min, and held at 280 °C for 3 min. The split ratio was set to 10:1 and the inlet temperature was 280 °C. Helium was used as the carrier gas with a flow rate of 1 mL/min. The ion source temperature and the interface temperature were set to 250 and 270 °C, respectively. A mass spectrometer was operated in electron ionization mode at an ionization voltage of 70 eV. A full scan from 35 to 600 $m/z$ was performed at a rate of 0.2 s/scan. The solvent removal time was 3 min. All samples were injected in sequence.

**5.5. Metabolite Identification and Quantitative Analysis.** Endogenous metabolites were identified using reference standards and by comparison with spectra from NIST 14, and the results were double-checked using the Human Metabolome Database[42] and Kyoto Encyclopedia of Genes and Genomes (KEGG).[43] Agilent ChemStation software was used to integrate the peak areas of the metabolites in each sample and normalize them to the peak area of the internal standard (2-isopropylmalate).

**5.6. Data Analysis and Identification of Potential Biomarkers.** The analytical results are presented as mean ± standard deviation. MATLAB (MathWorks Co.) software was used for further pattern analysis of metabolite information and potential biomarker discovery. A random forest (RF) algorithm was used to distinguish between samples from different groups. Details of the RF modeling process can be found elsewhere.[44] The RF algorithm combines classification and regression algorithms, which can deal with highly dimensional and correlated data sets without an initial dimensionality reduction of the data set. It provides two useful tools, a proximity matrix of the samples and the variable importance, which are helpful for data visualization and interpretation. The proximity matrix can be used to identify the underlying structure in data. Proximity values can be used to infer similarities among different samples. The proximity between two samples was calculated as the number of times that the two samples end up in the same terminal node of a tree, divided by the number of trees in the forest. After the proximity values were calculated, a multidimensional scaling plot was constructed, which can visualize the similarity or dissimilarity between samples.

An independent $t$-test was applied to detect significant differences in all metabolites between the two groups. A $P$-value of <0.05 was considered statistically significant.

**5.7. Network Pharmacology Analysis.** Through the Traditional Chinese Medicine Database and Analysis Platform (TCMSP; https://tcmspw.com/tcmsp.php), the chemical composition of XBJ, as well as potential drug targets was identified, and using OMIM (https://omim.org/), Genecards (https://www.genecards.org/), TTD (http://db.idrblab.net/ttd/), ParmGKB (https://www.pharmgkb.org/), and the DrugBank database (https://go.drugbank.com/), the collection targets for disease. The Venn Diagram Installation package of R×64 4.0.2 software was used to obtain the intersection targets of the identified drug and disease targets. Cytoscape 3.7.0 software was used to build an "active component−target−disease" network and the "NetworkAnalyzer" function was used to analyze its topological properties. Parameters including the value of the intermediate, centrality, and degree were derived. Intersection targets of drugs and diseases analyzed by a Venn diagram were imported into the STRING (https://string-db.org/) database to obtain the PPI protein interaction network. Using R×64 4.0.2 Bioconductor software combined with a bioinformatics database (https://bioconductor.org/), KEGG signal pathway enrichment analysis, and GO analysis, an intersection of drug and disease gene enrichment was performed, with $P < 0.05$ for selection criteria.

**5.8. Joint Pathway Analysis.** The targets from network pharmacology and the metabolites from plasma metabolomics were jointly analyzed to select crucial metabolic pathways by MetaboAnalyst (https://www.metaboanalyst.ca/).[45]

**5.9. Molecular Docking.** Active ingredients were selected from the PubChem database (https://pubchem.ncbi.nlm.nih.gov/), and the two-dimensional (2D) structure of the structure data file (SDF) format was obtained, analyzed by Chem3D software, and the compound space conformation was adjusted. The energy optimization was then minimized and the mol2 format was converted to a three-dimensional (3D) structure. The standard protein names of target genes were obtained from Uniprot data, and the 3D structure PDB files of AKT1, FOS, MAPK1, MAPK8, MAPK14, TNF, and JUN were downloaded from the PDB database (http://www1.rcsb.org/). PyMOLWin software was used to remove water molecules and small molecules. AutoDock Vina software was used for hydrogenation and format conversion of protein receptors. During the docking calculation, atomic charge and hydrogen atoms were added to the protein using an automatic docking tool. The auxiliary program AutoGrid was used to set up the docking box, and the docking box was defined according to the crystal structure of the protein complex of the known ligand. The Lamarckian genetic algorithm (LGA) was used in the docking process. Finally, PyMOLWin was used for visualization.



https://doi.org/10.1021/acsomega.1c02370
ACS Omega 2021, 6, 19717−19730

*5.9.1. Western Blot Analysis for Detection of Inflammation-Related Protein Expression.* Raw 264.7 cells were resuscitated and placed in Dulbecco's modified Eagle's medium (DMEM), a high glucose medium containing 10% fetal bovine serum and cultured in a constant temperature incubator at 37 °C and 5% $CO_2$. The cells were digested and passed with trypsin, and the logarithmic growth phase was used in the experiment. Raw 264.7 cells were randomly divided into blank, PQ, PQ + XBJ, and XBJ groups. The blank group was not treated, and the PQ and PQ + XBJ groups were treated with 600 $\mu$mol/L PQ for 24 h. The PQ + XBJ group was additionally treated with 10 and 20 $\mu$L/mL XBJ for 24 h. The XBJ group was treated with 10 and 20 $\mu$L/mL XBJ for 24 h.

The treated RAW 264.7 cells were placed on ice and treated with RIPA lysate for 30 minutes. And the cells were collected in EP tubes and centrifuged to obtain protein samples. The supernatant was taken and 5× sodium dodecyl sulfate (SDS) buffer was added at 95 °C for 5 min of thermostat heating denaturation and then centrifuged. The same amount of protein was separated by SDS−polyacrylamide gel electrophoresis (PAGE) and transferred to the poly(vinylidene difluoride) (PVDF) membrane after electrophoresis. Skim milk (5%) was added to Tris-buffered saline with Tween (TBST) buffer for 1 h at room temperature, followed by addition of p65 (1:1000), IKB$\alpha$ (1:1000), IKK$\beta$ (1:1000), p-p65 (1:1000), p-IKB$\alpha$ (1:1000), and p-IKK$\beta$ (1:1000) antibodies and internal $\beta$-actin (1:2000), and incubated in wave 4 °C incubation beds overnight. After washing the TBST film, the secondary antibody goat antirabbit IgG (1:4000) was added and incubated for 1 h. After washing the TBST film three times, a Chemidoc MP system was used to scan the strips, and Image Lab software was used to calculate the gray values.

## AUTHOR INFORMATION


### Corresponding Author

**Wen Liu** − *Department of Pharmacy, The First Affiliate Hospital of Hunan Normal University (Hunan Provincial People's Hospital), Changsha 410005, China*; Phone: +86-137-8701-7494; Email: liuwen@hunnu.edu.cn

### Authors

**Tongtong Wang** − *Department of Pharmacy, The First Affiliate Hospital of Hunan Normal University (Hunan Provincial People's Hospital), Changsha 410005, China*; orcid.org/0000-0001-7079-3390

**Sha Li** − *Department of Pharmacy, Changsha Stomatological Hospital, Changsha 410005, China*

**Yangke Wu** − *Department of Pharmacy, The First Affiliate Hospital of Hunan Normal University (Hunan Provincial People's Hospital), Changsha 410005, China*

**Xiao Yan** − *Department of Pharmacy, The First Affiliate Hospital of Hunan Normal University (Hunan Provincial People's Hospital), Changsha 410005, China*

**Yiming Zhu** − *Department of Pharmacy, The First Affiliate Hospital of Hunan Normal University (Hunan Provincial People's Hospital), Changsha 410005, China*

**Yu Jiang** − *Hunan Provincial Key Laboratory of Emergency and Critical Care Metabonomics, Changsha 410005, China*

**Feiya Jiang** − *Department of Pharmacy, The First Affiliate Hospital of Hunan Normal University (Hunan Provincial People's Hospital), Changsha 410005, China*

Complete contact information is available at: https://pubs.acs.org/10.1021/acsomega.1c02370

### Author Contributions

[‖]T.T.W. and S.L. contributed equally to this work.

### Notes

The authors declare no competing financial interest.


## ACKNOWLEDGMENTS

This work was supported by the Scientific Research Project of Hunan Provincial Commission of Health and Family Planning (no. B2017076), a research project with the Hunan Administration of Traditional Chinese Medicine (no. 201922) and the Foundation of Hunan Provincial Key Laboratory of Emergency and Critical Care Metabonomics. The authors would like to express their gratitude to EditSprings (https://www.editsprings.com/) for the expert linguistic services provided.

## REFERENCES


(1) Dinis-Oliveira, R. J.; Duarte, J. A.; Sánchez-Navarro, A.; Remião, F.; Bastos, M. L.; Carvalho, F. Paraquat poisonings: mechanisms of lung toxicity, clinical features, and treatment. *Crit. Rev. Toxicol.* **2008**, *38*, 13−71.

(2) Wang, Y.; Chen, Y.; Mao, L.; Zhao, G.; Hong, G.; Li, M.; Wu, B.; Chen, X.; Tan, M.; Wang, N.; Lu, Z. Effects of hemoperfusion and continuous renal replacement therapy on patient survival following paraquat poisoning. *PLoS One* **2017**, *12*, No. e0181207.

(3) Zhou, D.; Zhang, H.; Luo, Z.; Zhu, Q.; Zhou, C. Prognostic value of hematological parameters in patients with paraquat poisoning. *Sci. Rep.* **2016**, *6*, No. 36235.

(4) Veríssimo, G.; Bast, A.; Weseler, A. in vitroParaquat disrupts the anti-inflammatory action of cortisol in human macrophages: therapeutic implications for paraquat intoxications. *Toxicol. Res.* **2017**, *6*, 232−241.

(5) Wang, H.; Pan, J.; Shang, A.; Lu, Y. Time-dependent haemoperfusion after acute paraquat poisoning. *Sci. Rep.* **2017**, *7*, No. 2239.

(6) Hong, S.; Lee, J.; Sun, I.; Lee, K.; Gil, H. Prediction of patient survival in cases of acute paraquat poisoning. *PLoS One* **2014**, *9*, No. e111674.

(7) Gong, P.; Lu, Z.; Xing, J.; Wang, N.; Zhang, Y. Correction: Traditional Chinese medicine Xuebijing treatment is associated with decreased mortality risk of patients with moderate paraquat poisoning. *PLoS One* **2015**, *10*, No. e0130508.

(8) Wei, T. Y.; Yen, T. H.; Cheng, C. M. Point-of-care testing in the early diagnosis of acute pesticide intoxication: The example of paraquat. *Biomicrofluidics* **2018**, *12*, No. 011501.

(9) Liu, M.-w.; Su, M.-x.; Zhang, W.; Wang, Y.-q.; Chen, M.; et al. Protective effect of Xuebijing injection on paraquat-induced pulmonary injury via down-regulating the expression of p38 MAPK in rats. *BMC Complementary Altern. Med.* **2014**, *14*, No. 498.

(10) Xu, J.; Zhen, J.; Tang, L.; Lin, Q. Intravenous injection of Xuebijing attenuates acute kidney injury in rats with paraquat intoxication. *World J. Emerg. Med.* **2017**, *8*, 61−64.

(11) Gao, X.-J.; Xie, G.-N.; Liu, L.; Fu, Z.-J.; Zhang, Z.-W.; Teng, L.-Z. Sesamol attenuates oxidative stress, apoptosis and inflammation in focal cerebral ischemia/reperfusion injury. *Exp. Ther. Med.* **2017**, *14*, 841.

(12) Yin, Q.; Li, C. Treatment Effects of Xuebijing Injection in Severe Septic Patients with Disseminated Intravascular Coagulation. *Evidence-Based Complementary Altern. Med.* **2014**, *2014*, No. 949254.

(13) Ming, H.; Wu, W.; Jian, G.; Li, Y. The interventional effect of Xuebijing injection on expression of mitochondrial fusion protein 2 and the ultrastructure changes in lung tissues in rats with paraquat poisoning. *Zhonghua Weizhongbing Jijiu Yixue* **2014**, *26*, 388−393.

(14) Gong, P.; Lu, Z.; Xing, J.; Wang, N.; Zhang, Y. Traditional Chinese Medicine Xuebijing Treatment Is Associated with Decreased

Mortality Risk of Patients with Moderate Paraquat Poisoning. *PLoS One* **2015**, *10*, No. e0123504.
(15) Li, X. Y.; Du, B.; Wang, Y. S.; Kang, H. Y. J.; Tong, Z. H. The keypoints in treatment of the critical coronavirus disease 2019 patient. *Zhonghua Jiehe He Huxi Zazhi* **2020**, *43*, 277.
(16) Chen, L.; Cao, Y.; Zhang, H.; Lv, D.; Zhao, Y.; Liu, Y.; Ye, G.; Chai, Y. Network pharmacology-based strategy for predicting active ingredients and potential targets of Yangxinshi tablet for treating heart failure. *J. Ethnopharmacol.* **2018**, 359.
(17) Liu, Z. H.; Sun, X. B. Network pharmacology: new opportunity for the modernization of traditional Chinese medicine. *Yaoxue Xuebao* **2012**, *47*, 696−703.
(18) Deng, M.; Zhang, M.; Sun, F.; Ma, J.; Hu, L.; et al. A Gas Chromatography-Mass Spectrometry Based Study on Urine Metabolomics in Rats Chronically Poisoned with Hydrogen Sulfide. *BioMed Res. Int.* **2015**, *2015*, No. 295241.
(19) Fiehn, O. Metabolomics by Gas Chromatography-Mass Spectrometry: Combined Targeted and Untargeted Profiling. *Curr. Protoc. Mol. Biol.* **2016**, *114*, 21.33.1−21.33.11.
(20) Wen, C.; Wang, Z.; Zhang, M.; Wang, S.; Geng, P.; Sun, F.; Chen, M.; Lin, G.; Hu, L.; Ma, J.; Wang, X. Metabolic changes in rat urine after acute paraquat poisoning and discriminated by support vector machine. *Biomed. Chromatogr.* **2016**, *30*, 75−80.
(21) Hadi, N. I.; Jamal, Q.; Iqbal, A.; Shaikh, F.; et al. Serum Metabolomic Profiles for Breast Cancer Diagnosis, Grading and Staging by Gas Chromatography-Mass Spectrometry. *Sci. Rep.* **2017**, *7*, No. 1715.
(22) Ren, Y.; Yao, M.; Huo, X.; Gu, Y.; Zhu, W.; Qiao, Y.; Zhang, Y. Study on treatment of "cytokine storm" by anti-2019-nCoV prescriptions based on arachidonic acid metabolic pathway. *Zhongguo Zhongyao Zazhi* **2020**, *45*, 1225−1231.
(23) Dam, G.; Aamann, L.; Vistrup, H.; Gluud, L. L. The role of Branched Chain Amino Acids in the treatment of hepatic Encephalopathy - ScienceDirect. *J. Clin. Exp. Hepatol.* **2018**, *8*, 448−451.
(24) Ruiz-Ramírez, A.; Ortiz-Balderas, E.; Cardozo-Saldaña, G.; Diaz-Diaz, E.; El-Hafidi, M. Glycine restores glutathione and protects against oxidative stress in vascular tissue from sucrose-fed rats. *Clin. Sci.* **2014**, *126*, 19−29.
(25) Strumpf, I. J.; Drucker, R. D.; Anders, K. H.; Cohen, S.; Fajolu, O. Acute eosinophilic pulmonary disease associated with the ingestion of L-tryptophan-containing products. *Chest* **1991**, *99*, 8−13.
(26) Edamatsu, T.; Fujieda, A.; Itoh, Y. Phenyl sulfate, indoxyl sulfate and p-cresyl sulfate decrease glutathione level to render cells vulnerable to oxidative stress in renal tubular cells. *PLoS One* **2018**, *13*, No. e0193342.
(27) Praschberger, M.; et al. The uremic toxin indoxyl sulfate acts as a pro- or antioxidant on LDL oxidation. *Free Radical Biol. Med.* **2014**, *75*, S36.
(28) Zang, L. Y.; Kuijk, F. J. V.; Misra, H. P. EPR studies of spin-trapped free radicals in paraquat-treated lung microsomes. *Biochem. Mol. Biol. Int.* **1995**, *37*, 255−262.
(29) Lei, S.; Zavala-Flores, L.; Garcia-Garcia, A.; Nandakumar, R.; Huang, Y.; Madayiputhiya, N.; Stanton, R. C.; Dodds, E. D.; Powers, R.; Franco, R. Alterations in Energy/Redox Metabolism Induced by Mitochondrial and Environmental Toxins: A Specific Role for Glucose-6-Phosphate-Dehydrogenase and the Pentose Phosphate Pathway in Paraquat Toxicity. *ACS Chem. Biol.* **2014**, *9*, 2032−2048.
(30) Baron, J. A.; Laws, K. M.; Chen, J. S.; Culotta, V. C. Superoxide Triggers an Acid Burst in Saccharomyces cerevisiae to Condition the Environment of Glucose-starved Cells*. *J. Biol. Chem.* **2013**, *288*, 4557.
(31) Bangera, M.; Giri, G. K.; Sagurthi, S. R.; Murthy, M. R. N. Structural and functional insights into phosphomannose isomerase: the role of zinc and catalytic residues. *Acta Crystallogr., Sect. D: Struct. Biol.* **2019**, 475.
(32) Wetmore, D. R.; Joseloff, E.; Pilewski, J.; Lee, D. P.; Lawton, K. A.; Mitchell, M. W.; Milburn, M. V.; Ryals, J. A.; Guo, L. Metabolomic Profiling Reveals Biochemical Pathways and Biomarkers Associated with Pathogenesis in Cystic Fibrosis Cells. *J. Biol. Chem.* **2010**, *285*, 30516−30522.
(33) Laguna, T. A.; Reilly, C. S.; Williams, C. B.; Welchlin, C.; Wendt, C. H. Metabolomics analysis identifies novel plasma biomarkers of cystic fibrosis pulmonary exacerbation. *Pediatr. Pulmonol.* **2015**, *50*, 869−877.
(34) Shang, V. C. M.; O'Sullivan, S. E.; Kendall, D. A.; Roberts, R. E. The endogenous cannabinoid anandamide increases human airway epithelial cell permeability through an arachidonic acid metabolite. *Pharmacol. Res.* **2016**, 152.
(35) Leuti, A.; Maccarrone, M.; Chiurchiù, V. Proresolving Lipid Mediators: Endogenous Modulators of Oxidative Stress. *Oxid. Med. Cell. Longevity* **2019**, *2019*, 1−12.
(36) Wen, Y.; Gu, J.; Chakrabarti, S.; Aylor, K.; Marshall, J.; Takahashi, Y.; Yoshimoto, T.; Nadler, J. The role of 12/15-lipoxygenase in the expression of interleukin-6 and tumor necrosis factor-alpha in macrophages. *Endocrinology* **2007**, *148*, 1313−1322.
(37) Li, Z.; Li, J.; Zhang, F.; Zhu, N.; Hou, J. Antidiarrheal Effect of Sechang-Zhixie-San on Acute Diarrhea Mice and Network Pharmacology Deciphering Its Characteristics and Potential Mechanisms. *Evidence-Based Complementary Altern. Med.* **2020**, *2020*, No. 8880298.
(38) Wen, Y.; Gu, J.; Chakrabarti, S. K.; Aylor, K.; Marshall, J.; et al. The role of 12/15-lipoxygenase in the expression of interleukin-6 and tumor necrosis factor-alpha in macrophages. *Endocrinology* **2007**, *148*, 1313−1322.
(39) Vallabhapurapu, S.; Karin, M. Regulation and Function of NF-B Transcription Factors in the Immune System. *Annu. Rev. Immunol.* **2009**, *27*, 693−733.
(40) Sarri, B.; Poizat, F.; Heuke, S.; Wojak, J.; Franchi, F.; et al. Stimulated Raman histology: one to one comparison with standard hematoxylin and eosin staining. *Biomed. Opt. Express* **2019**, *10*, 5378.
(41) Zhou, X.; Wang, Y.; Yun, Y.; Xia, Z.; Lu, H.; et al. A potential tool for diagnosis of male infertility: Plasma metabolomics based on GC−MS. *Talanta* **2016**, 82.
(42) Wishart, D. S.; Feunang, Y. D.; Guo, A. C.; Lo, E. J.; Marcu, A.; Grant, J. R.; Sajed, T.; Johnson, D.; Li, C.; Sayeeda, Z.; et al. DrugBank 5.0: a major update to the DrugBank database for 2018. *Nucleic Acids Res.* **2018**, *46*, D1074.
(43) Kanehisa, M.; Araki, M.; Goto, S.; Hattori, M.; Hirakawa, M.; et al. KEGG for linking genomes to life and the environment. *Nucleic Acids Res.* **2008**, *36*, D480−D484.
(44) Chen, T.; Cao, Y.; Zhang, Y.; Liu, J.; Bao, Y.; Wang, C.; Jia, W.; Zhao, A. Random Forest in Clinical Metabolomics for Phenotypic Discrimination and Biomarker Selection. *Evidence-Based Complementary Altern. Med.* **2013**, *2013*, No. 298183.
(45) Li, X.; Qin, X.; Tian, J.; Gao, X.; Du, G.; Zhou, Y. Integrated network pharmacology and metabolomics to dissect the combination mechanisms of Bupleurum chinense DC-*Paeonia lactiflora* Pall herb pair for treating depression. *J. Ethnopharmacol.* **2021**, *264*, No. 113281.


https://doi.org/10.1021/acsomega.1c02370
*ACS Omega* 2021, 6, 19717−19730